

On the influence of the intermolecular potential on the wetting properties of water on silica surfaces

E. Pafong,¹ J. Geske,¹ and B. Drossel¹

Institut für Festkörperphysik, Technische Universität Darmstadt, Hochschulstr. 6, 64289 Darmstadt, Germany^{a)}

(Dated: 23 June 2016)

We study the wetting properties of water on silica surfaces using molecular dynamics (MD) simulations. To describe the intermolecular interaction between water and silica atoms, two types of interaction potential models are used: the standard Bródka and Zerda (BZ) model, and the Gulmen and Thompson (GT) model. We perform an in-depth analysis of the influence of the choice of the potential on the arrangement of the water molecules in partially filled pores and on top of silica slabs. We find that at moderate pore filling ratios, the GT silica surface is completely wetted by water molecules, which agrees well with experimental findings, while the commonly used BZ surface is less hydrophilic and is only partially wetted. We interpret our simulation results using an analytical calculation of the phase diagram of water in partially filled pores. Moreover, an evaluation of the contact angle of the water droplet on top of the silica slab reveals that the interaction becomes more hydrophilic with increasing slab thickness and saturates around 2.5 – 3 nm, in agreement with the experimentally found value. Our analysis also shows that the hydroaffinity of the surface is mainly determined by the electrostatic interaction, but that the van der Waals interaction nevertheless is strong enough that it can turn a hydrophobic surface into a hydrophilic surface.

I. INTRODUCTION

Water is an essential material in our everyday life and is the most used solvent for chemical and biological reactions. Water molecules are highly polar, forming hydrogen-bonded networks and sharing hydrogen bonds with other molecules. In particular, water confined within nanoscale geometries of hydrophilic surfaces is subject to two competing interactions: the hydrophilic interactions between water molecules and those between water and surface molecules.

One of the standard systems for studying hydrophilic interactions with water are silica nanopores such as sols-gels,¹ mesoporous silica (MCM-41),^{2–7} Vycor-glasses,^{8–10} controlled pore glasses (CPG).^{11–15} Water confined in silica nanopores or near silica flat surfaces is a topic which has attracted considerable attention,^{16–22} mainly because of the relevance of the water-silica interaction in understanding water transport in porous rocks,²³ nanofluidic devices,²⁴ heterogeneous catalysis in mesoporous materials,^{15,25} and permeation through membrane channels.²⁶ Experimental investigations of water in silica nanopores have been carried out using NMR spectroscopy,^{2,12} X-ray and neutron diffraction,^{5,6,9,10,27,28} quasi-elastic neutron scattering,^{3,4} Small-angle neutron scattering (SANS),⁸ and optical Kerr-effect spectroscopy,¹ showing that the dynamics of water in such pores is slow in comparison to the dynamics of bulk water. This originates from the strong binding or trapping of water molecules by silica surfaces as found by experimental measurements conducted with MCM-41

as well as CPG pores^{2,12} resulting in a complete coverage of the pore surface at even moderate hydration levels. Accordingly, the intermolecular interactions between water and silica surfaces in MD simulations should be set up such that the experimental results are reproduced.

The influence of the filling ratios on the wetting properties of water in silica nanopores has been studied by previous MD research.^{29–32} Such investigations are motivated by the fact that in experiments the fluid is placed on top of a porous surface and flows to enter the pores. In the mentioned MD simulations, it was demonstrated that at all hydration levels water molecules are absorbed by the Vycor material. However, they have not shown to what extent the pore surface is wetted, whether it is only partially wetted or rather completely wetted (as expected from measurements^{2,12}). Moreover, the confinement near such hydrophilic surface was found to substantially alter the dynamic behaviour of water, depending on the filling ratio^{19,33}, but it has not been checked how this relates to the configurations that water can take inside the pore. In all these previous MD analyses, the (12-6) Lennard-Jones (LJ) potential and the partial charges assigned to each silica atom site are chosen according to Bródka and Zerda (BZ).³⁴ In this model, the LJ potential parameters for silica oxygen atoms are approximated from the Kirkwood-Mueller formula³⁵, while no LJ interaction centers are assigned to silicon and hydrogen (of the silanol groups) as they are small in size and possess a low polarizability. In the present investigation, we have found that water molecules do not completely wet the BZ silica model surface at intermediate hydration levels. For this reason, the silica model recently introduced by Gulmen and Thompson³⁶ (GT) has been tested. The GT³⁶ potential is defined similarly to the silica potential

^{a)}priscel@fkp.tu-darmstadt.de

by BZ,³⁴ however, a weak short-ranged interaction for silicon and hydrogen atoms has been added and the partial charges on each silica atom are increased. We probed the performance of both silica models by analyzing the wetting behaviour of water on silica surfaces and comparing to the experimental results.^{2,12,37–39}

In the following, we present the results of MD simulations of water in a cylindrical silica nanopore of roughly 4 nm diameter and 6.1 nm height. Additionally, MD simulations of water droplets wetting silica slabs of varying thicknesses were performed. The silica nanopores and slabs were created in our group, with the silanols molecules uniformly distributed on the surface. For water in the silica pore, we evaluate the minimum number of water layers necessary to completely wet a silica surface by looking at the radial and angular density distribution, as well as the number of hydrogen bonds formed for different filling ratios of water in the pore. Furthermore, a phase diagram of the surface tension of the different configurations adopted by water molecules in the nanopore is calculated analytically, providing deeper insights into the relation between the interaction energies and the water arrangement in the pore.

To complete the work, the contact angle of a water droplet on a silica flat slab is evaluated and compared between the two model surfaces. Previous MD investigations have used the contact angle investigation to approximate LJ parameters between water and silica atoms^{40,41} but they have not stated clearly whether the simulations were performed in such a way that the periodic images provided by the periodic boundary conditions do not influence the contact angle evaluated. In our investigation, we run the simulations without periodic boundary conditions to avoid this issue. Previous experimental results showed that the wetting properties do not only involve atoms of layers in the vicinity of the interface but also the atoms located deeply inside the slab material.^{37–39,42} Therefore, we measure how the contact angle changes with the thickness of the slab, showing that a thickness of 2.5–3 nm is sufficient for MD simulations. In order to disentangle the contributions of the interfacial electrostatic and van der Waals (VdW) interactions on the contact angle, we varied these two contributions in our simulations, showing that the influence of the electrostatic interaction is considerably larger than that of the VdW interaction.

II. SIMULATION DETAILS

Classical MD simulations were performed with the NAMD⁴³ 2.10 simulation package. An amorphous cylindrical nanopore of roughly 4 nm of diameter and silica slabs of different thicknesses were fabricated in our group. To create the pore, a crystalline cell of SiO₂ with a box length of approximately 6 nm was built, the system was melted at 5000 K and cooled to room

temperature with the method described in⁴⁴, and then a cylindrical cavity of ~ 4 nm diameter was cut. The process of fabrication of the silica cylindrical pore and the silica slab is explained in detail in a separate paper.⁴⁴ The surface concentration of hydroxyl groups on the surface is 7.5 nm^{-2} corresponding to highly hydrated silica surfaces.³⁴ The silica slabs were created following a similar procedure.

The silica nanopore and slab contain two types of oxygen atoms depending on the number of silicon atoms to which they are connected. There are bridging oxygens (O_{Si}) bonded to two adjacent silicons and nonbridging oxygens (O_H) on the surface attached to only one silicon. Hydrogen atoms are attached to the O_H in order to form the silanols groups (SiOH, Si(OH)₂). The bonded interaction parameters for silica atoms were obtained from Hill and Sauer.⁴⁵ Apart from the hydrogen atoms of the silanols groups that are allowed to rotate, all atoms in the silica pore and slab are immobile, constrained to a fixed position. Whereas, water molecules are free to move within the pore. Liquid water is defined using 2 models: a set of 3 rigid sites given by the SPC/E⁴⁶ model and a set of 4 sites provided by the TIP4P2005⁴⁷ model. The atoms of the silica substrate are allowed to interact with the water sites by means of the Coulomb potential and LJ potential in Eq. (1),

$$U_{\text{LJ}} = 4\epsilon \left(\frac{\sigma_{i,j}^{12}}{r_{i,j}^{12}} - \frac{\sigma_{i,j}^6}{r_{i,j}^6} \right) \quad (1)$$

which implements the VdW interaction. LJ parameters and fractional charges for the SiO₂ sites are given in Table I.

All simulations were made with the NVT ensemble with a fixed room temperature $T = 298$ K using a Langevin thermostat⁴³ with a coupling coefficient of 1.0 ps^{-1} and with the hydrogen atoms included in the Langevin dynamics. An integration time step of 2 fs was utilized and the simulations were run for at least 20 ns. Periodic boundary conditions were set for the simulations of water in the nanopore allowing the calculation of the long-range Coulombic electrostatic interactions with the particle-mesh Ewald sum, using a cut-off of 1.2 nm. No periodic boundary conditions were defined for the simulation of water wetting silica slabs in order to allow the calculation of the full electrostatic and VdW interactions between all the water droplet atoms and silica slab atoms.

III. RESULTS I: WATER IN PARTIALLY FILLED SILICA PORES

In the following, we investigated the configuration of water in a partially filled silica pore for the two different models using MD simulations. Furthermore, we performed an analytical calculation of the different possible

TABLE I. LJ potential parameters for silica interaction centers. *values were not mentioned in the model and were chosen arbitrarily small.

Parameters	Sites	σ (nm)	ϵ (Kcal/mol)	q (e)
BZ ³⁴	Si	0.0178*	0.00000	1.283
	O _{Si}	0.27	0.45705694	-0.629
	O _H	0.3	0.45705694	-0.533
	H	0.0178*	0.00000	0.206
GT ³⁶	Si	0.25	0.0001	1.28
	O _{Si}	0.27	0.457	-0.64
	O _H	0.307	0.17	-0.74
	H	0.1295	0.0003657	0.42

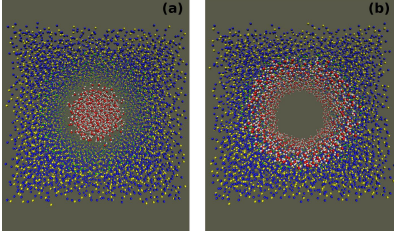


FIG. 1. Top view of the two initial configurations used in the MD simulations, labelled in the subsequent figures with "center" (a) and "surface" (b). Here the hydration level is 30%. Si, O_{Si,H}, H are drawn in yellow, blue and green, while water atoms O, H are indicated by red and white respectively. The pictures were generated using the VMD program.⁴⁸

phases of water in a cylindrical pore that allows us to interpret the findings.

A. MD simulation results

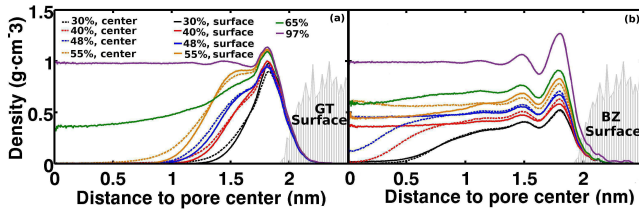


FIG. 2. Radial density profile of water in the silica pore for different filling ratios and starting configurations, for the (a) BZ surface and the (b) GT surface. The radius of the pore is 2 nm. The gray area indicates the silica pore surface and is arbitrarily scaled for a clear visibility.

We evaluated the equilibrated configurations of water in the pore for the GT and BZ surfaces, using different filling ratios and different starting configurations. The pore filling ratios are in the range 30% - 97%, based on the estimated number of molecules for 100% filling ratio, which is 2700.³⁰ The equilibrium configurations

were analyzed by calculating the radial density profile, the distribution of water molecules on the interior pore surface, and the number of hydrogen bonds among water molecules and between water and silica molecules. In order to see how far the final configurations depend on the initial configuration, we used the two different initial configurations shown in Fig. 1, where water is concentrated around the cylinder axis and at the pore surface, respectively. There is thus a void between the water droplet and the silica surface in the first configuration, and a void in the pore center for the second configuration. Fig. 2 shows the radial density profile of water molecules inside the pore as function of the distance to the pore center, averaged over 15 ns after at least 5 ns of equilibration for each simulation. One can see that water is closer to the GT surface. The GT density profile shows only one peak for a filling ratio of 30%, indicating that all water molecules are in contact with the pore surface. Only after the first layer is completed, a second layer is formed, as is visible for the curves for filling ratios between 40 and 55%. At 65% filling ratio, the water molecules can also be found in the interior of the pore, indicating a configuration with a completely wetted surface and a compact water droplet in the pore interior. The density profiles for

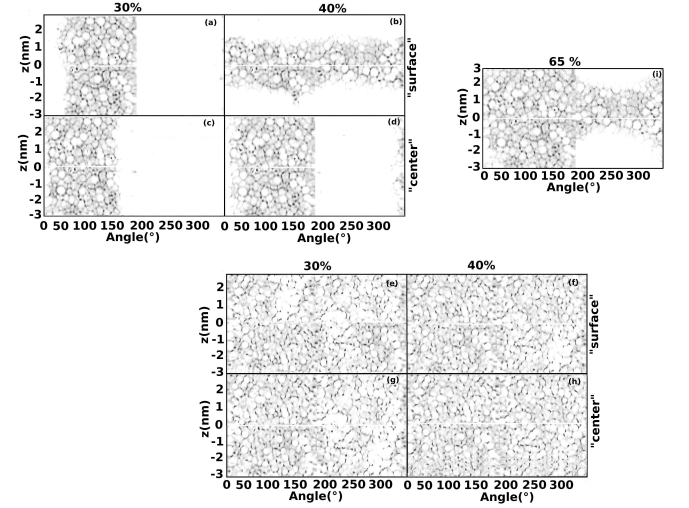


FIG. 3. The water density at the pore surface, showing water molecules that are within a distance of 0.3 nm of the silica surface. For the GT surface (e-h), only filling ratios of 30 and 40% are shown, since for larger filling ratios the surface is completely wetted. For the BZ surface, the top (a-b) graphs correspond to the "surface" starting configuration and the bottom graphs (c-d) correspond to the "center" starting configuration, (i) represents the density at 65% filling ratio.

the BZ surface show several layers of water, with a peak height that depends on the filling ratio. Furthermore, the density profile depends on the initial configuration for intermediate filling ratios, with the initial configurations at the surface leading to final configurations with rather flat density profiles. This suggests that for the initial configu-

ration at the boundary, the water droplet forms a "plug" in the pore interior, while for the initial configuration in the center, water forms some type of droplet sitting at the surface. Since the pore surface is rough, some water molecules can also be found inside the silica pore material.

In order to test the intuition obtained for the water configurations based on the density profiles, we evaluated the distribution of water molecules within a distance of 0.3 nm of the surface. Fig. 3 shows the resulting surface density profiles, using cylinder coordinates. This figure confirms that for the GT surface, the water droplet first wets the surface completely, before filling the interior. For the BZ surface, the pore surface is only partially covered with water, and the final configuration depends on the starting configuration for intermediate filling ratios. For instance, for 40% filling ratio with the "center" starting configuration, water molecules are concentrated in one angular segment of the surface but are covering the whole length, while for the "surface" starting configuration they occupy only part of the z range, but all angles. These final configurations for intermediate filling ratios are in fact very plausible if one tries to imagine how the initial configurations can evolve with time in a situation where the water-surface interaction is not strong enough that the entire surface is wetted. When the initial configuration has a water cylinder in the pore center, the entire cylinder gets attracted by the silica molecules under the influence of electrostatic and VdW interaction and moves as a whole towards the pore surface, wetting a specific angular region of the surface. When the initial configuration sits at the pore surface, the water film may rupture along an angular line, and the water will contract to form a plug. Even if one of the two final configurations has a lower free energy, this free energy difference will not be large, and the transition between them will involve a barrier that is so large that it is not overcome during the simulation time. When the filling ratio is lower (as can be seen for 30%), the plug is not observed for either initial configuration, indicating that there is only one stable configuration. The two different final configurations merge also for larger filling ratios (as can be seen for 65%), where the void left by the water droplet takes the shape of a droplet that sits at the pore surface.

Finally, we evaluated the average number of hydrogen bonds formed between water molecules, and between water molecules and silica molecules. This shows to what extent the stronger hydroaffinity of the GT model affects the formation of molecular bonds. We considered two oxygen atoms to be connected via a hydrogen bond if the angle between the intramolecular O-H vector and the intermolecular O...O vector is less than 30° , provided that the O...O separation is less than 0.335 nm. The results are shown in Fig. 4. For the BZ surface, the number of hydrogen bonds between water molecules reaches the bulk value in the inner part of the pore for a filling ratio larger than 40% with the "surface" initial configuration.

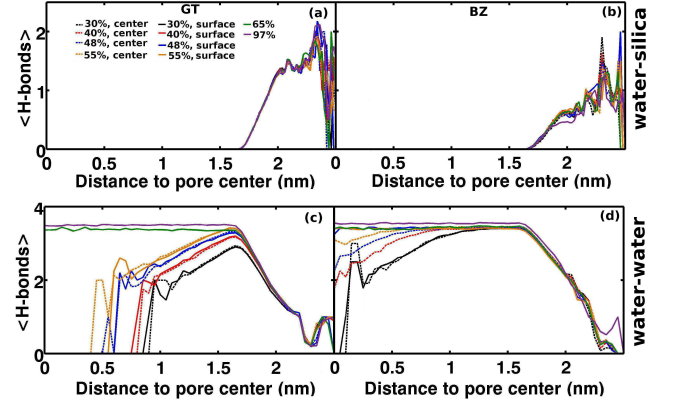


FIG. 4. Average number of hydrogen bonds per water molecules for water-silica (a-b) and water-water (c-d) contacts, for different initial conditions and filling ratios, as indicated in the legends. The results for the GT silica surface are given on the left-hand side, and those for the BZ silica surface on the right-hand side.

Also for the "center" initial condition, the bulk value is reached for the water molecules in the interior of the water droplet. In the GT surface, the bulk value is reached only for filling ratios above 60%. This illustrates the fact that the BZ surface disrupts the water structure more than the GT surface. Accordingly, the number of hydrogen bonds formed between the silica surface and the water molecules is larger for the GT surface.

For both models, the maximum number of water-silica hydrogen bonds is already reached at 40% filling ratio, confirming that one and half layer of water molecules is sufficient to completely wet the GT silica surface. It is at first surprising that for the BZ surface, the number of water-silica hydrogen bonds does not increase for filling ratios larger 40% and stays considerably below the value of the GT surface. This can only be explained by different water orientations near the surface in the two models. In the supplementary information we show that near the BZ surface the OH bonds of water molecules have a preferred orientation, while this is not the case near the GT surface. This means that only part of the water molecules can act as a hydrogen bond donor or acceptor near a BZ silica molecule, while near the GT surface all the water molecules can share hydrogen bonds with the surface atoms.

B. Theoretical evaluation of the phase diagram

In order to better understand the dependence of the water droplet configuration in the pore on the interaction energies and the filling ratio, we performed a theoretical analysis that is based on surface energy minimization. Denoting the surface area between the water droplet and vacuum with A_1 , the surface area between

the water droplet and the pore material with A_2 , and γ_1 as the surface tension between water and vacuum, γ_2 as the difference between the surface tension of silica and water with the surface tension of silica and vacuum. The total surface energy of the wetting droplet can be written as

$$E_S = \gamma_1 \cdot A_1 + \gamma_2 \cdot A_2. \quad (2)$$

If we assume that the entropy does not change much between different phases, the configuration of the water droplet in the pore can be obtained by minimizing E_S for a given filling ratio. In order to perform the calculation mostly analytically, we approximated the different possible phases using simple geometrical shapes, so that the energy minimization can be performed by varying at most 2 parameters that characterize the phase. We fixed the ratio of the pore radius and pore length to the value $R/L = 2/6.1$ used in the simulations. We determined the phase diagram in dependence of the filling ratio and the ratio between the two surface energies. We allowed for hydrophilic ($\gamma_2 < 0$) as well as for hydrophobic surfaces ($\gamma_2 > 0$). The surface tension γ_1 is a positive quantity.

Fig. 5 shows the eight phases and the phase diagram obtained from minimizing E_S .

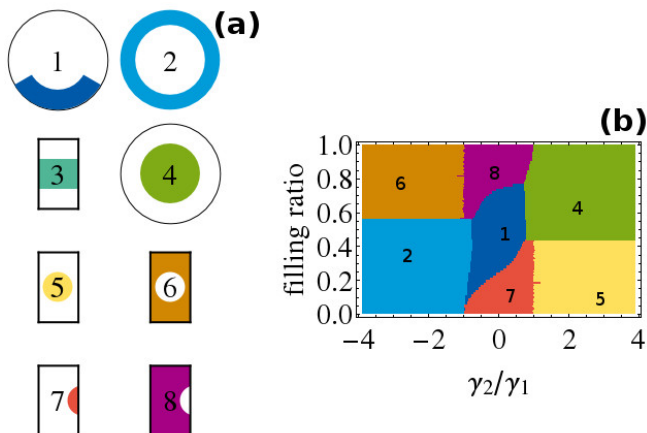


FIG. 5. (a) The eight different phases used for energy minimization and (b) the phase diagram in dependence of the ratio of the water-vacuum and water-silica surface energies and of the filling ratio. The aspect ratio between radius and length of the cylindrical pore is $2/6.1$.

Phases 1, 2, and 4 are translationally invariant along the cylinder axis and represent the cases of partial, full, and no wetting of the silica surface. Phase 3 represents a plug in the shape of a cylinder that is shorter than the pore. Phases 5-8 describe the cases where the water or the vacuum forms a spherical droplet in the interior or one that intersects with the pore surface.

The calculation of the surface energy for phases 1-6 is a straightforward analytical calculation. For phase 1, we had to use mathematica to evaluate the final expression. In order to evaluate phases 7 and 8, we had to resort

to a numerical evaluation. We first created a data base by calculating numerically the volume and surface of the cut droplet for over 1 million different combinations of the sphere radius and the distance of the sphere center from the cylinder axis. Then, we used this data base to find for a given filling ratio the values that minimize E_S .

The phase diagram shows clearly three qualitatively different regions that depend on the ratio γ_2/γ_1 . For $\gamma_2/\gamma_1 \lesssim -1$, the energy is minimized by having maximum surface area with the pore surface. The water wets the pore completely. Correspondingly, the phases 2 and 6 occur. With increasing filling ratio, the volume of the vacuum becomes smaller, and eventually a free volume that does not touch the surfaces fits into the pore. For sufficiently large filling ratio, a droplet clearly has the smaller surface area with the vacuum and therefore the lower energy. (Our simple calculation did not take into account that the droplet could be stretched, and therefore the position of the phase boundary between phases 2 and 6 should in fact be at a lower filling ratio.)

For $\gamma_2/\gamma_1 \gtrsim 1$, the pore material is highly hydrophobic, and the phases 4 and 5, which have no contact between water and silica, have the lowest energy, depending on the filling ratio.

In the intermediate parameter region $-1 \lesssim \gamma_2/\gamma_1 \lesssim 1$, we observe phases 7, 1, and 8 as the filling ratio is increased. These are the phases that have surfaces with the pore and with the vacuum. Since the (absolute value of) water-vacuum energy is larger than that of the water-silica energy, these phases are to a large extent affected by the condition that the water-vacuum interface shall be minimum. The transition from phase 7 to phase 1 occurs for lower values of γ_2/γ_1 at smaller filling ratios than for larger γ_2/γ_1 , because a larger surface area to the pore is energetically favorable for negative γ_2 . For the same reason, phase 8 wins over phase 1 for high filling ratios and negative γ_2 , because phase 8 has more surface area between water and the pore.

Phase 3 does not occur in the phase diagram. It will certainly occur when the ratio between radius and length of the pore becomes smaller, because it has then smaller surface areas than phase 1. In our simulations with the BZ potential, we found this phase for intermediate filling ratios, where it coexists with phase 1. Phase 3 thus might well be metastable. On the other hand, it is also possible that phase 3 is indeed stable in part of the phase diagram due to entropic effects, which were not taken into account when calculating the phase diagram. Since in the canonical NVT ensemble the free energy $F = E - TS$ has to be minimized, phases with larger entropy become more favored when entropy is taken into account. This will shift the phase boundaries somewhat. For instance, when phase 2 contains only two layers of water molecules, its entropy per molecule is smaller than in bulk water. Similarly, the entropy per water molecule is larger in phase 3 than in phase 1, since the water in phase 3 is more bulk-like.

With the insights gained from these analytical calcu-

lations, we can interpret the results of the MD simulations: For the BZ surface, the water wetted the silica surface only partially for all simulated filling ratios, and we observed the phases 1, 3, and 8 depending on the filling ratio. This means that the ratio of surface energies in the interval $\gamma_2/\gamma_1 \in (-1, 0)$. (Since the surface is hydrophilic, we have $\gamma_2 < 0$.) With the GT surface, we observed a complete wetting of the silica surface (phases 2 and 6) for all simulated filling ratio, which means that $\gamma_2/\gamma_1 < -1$. This appears to be the more realistic scenario, as it agrees well with experimental results.²

In order to obtain an additional perspective on the different interaction between water and a silica surface in the two models, we will in the next section investigate the contact angle of water on top of a flat silica slab using both models.

IV. RESULTS II: WATER ON TOP OF A SILICA SLAB

A good tool to examine the performance of silica potentials is the evaluation of the contact angle of a water droplet wetting the surface. We performed MD simulations of a water droplet on a flat surface of amorphous silica and measured the contact angle. We did not use periodic boundary conditions in order to remove the influence of the neighbouring water periodic images. Instead, the Coulombic and the VdW (LJ) interaction energies between all atoms in the water droplet and the silica slab were calculated exactly.

In order to evaluate the contact angle θ , the density profile of all horizontal water layers of 0.05 nm thickness was determined, and from these a contour plot of the density was obtained. The contour plot was fitted to a circular segment, and the contact angle was deduced from the tangential line to the base of the circular segment. The result is shown in Fig. 6 for both types of potentials, with a slab of thickness $t = 2.5$ nm. For the GT model, the droplet covers the entire surface and has a very small contact angle of 7° . When we performed the same simulation with periodic boundary conditions, the water layer became completely flat. In contrast, the contact angle of the water droplet on top of the BZ surface is 25° . These results confirm the findings of the previous subsection, that the GT silica surface is so hydrophilic that water wets it completely, while the BZ surface is less hydrophilic.

The contact angle is closely related to the surface tensions that we used for evaluating the phase diagram. The condition that the total surface energy (E_s) of water wetting a silica surface must be minimal for an equilibrated droplet of constant volume, i.e., $dE_s = 0$, leads to

$$\frac{dA_1}{dA_2} = -\frac{\gamma_2}{\gamma_1} = \cos \theta. \quad (3)$$

The contact angle of 25° for the BZ surface agrees with our conclusion that $-1 < \gamma_2/\gamma_1 < 0$ and leads more precisely to $\gamma_2/\gamma_1 \simeq -0.9$. For the GT surface, we had

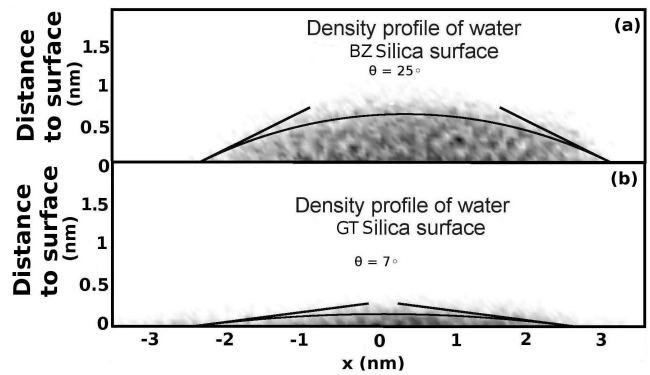


FIG. 6. Contact angle of a water droplet on top of a silica slab of thickness $t = 2.5$ nm. (a) and (b) correspond respectively to the BZ and the GT silica surface.

obtained that $\gamma_2/\gamma_1 < -1$, implying a contact angle of zero and complete wetting, which is compatible with our finding that the droplet spreads on the surface forming only the 1.5 layers required for wetting.

Our finding of a very small contact angle for the BZ surface is in agreement with what is found in experiments.³⁷⁻³⁹ In those experiments, the precise value of the angle depends on whether the advancing or receding droplet is considered, and on the thickness of the slab, and it ranges from 0° to 7° .

Since the interaction strength between water and silica is known to depend on the thickness of the slab^{37-39,42}, we evaluated the contact angle for different values of the thickness t (within the GT model), see Fig. 7. The cosine of the contact angle increases with thickness and reaches its limit when $t = 2.5$ nm, where the contact angle is $\approx 7^\circ$. A similar dependence of the cosine of the contact angle on thickness has been measured.³⁷ It means that, to accurately reproduce the wetting properties of a water droplet on a silica slab, the slab should have at least a thickness in the range 2.5-3 nm. This result is close to the experimental value 3 nm found by Williams and Goodman.³⁷ The change of the contact angle with

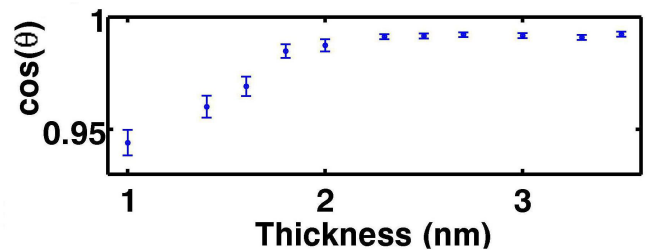


FIG. 7. Dependence of the cosine of the contact angle θ of the water droplet on the thickness of the silica slab. The MD simulation was done with the GT model, using 469 water molecules.

thickness shows also that water does not wet the surface

completely when the slab is thin. This means that the ratio γ_2/γ_1 changes from a value > -1 to a value < -1 with increasing thickness, implying that this ratio is very close to -1 . This in turn means that small differences in the preparation of the surface can shift the ratio over the threshold -1 , and this may explain why some experiments find a nonzero contact angle, while others find complete wetting.

	ϵ_{GT}, q_{GT}	$1\%\epsilon_{GT}, q_{GT}$	$\epsilon_G, (q = 0)$
$t = 1.6 \text{ nm}$	14.3°	17.2°	105°
$t = 2.0 \text{ nm}$	9.0°	12.3°	88°
$t = 2.5 \text{ nm}$	7.0°	11.1°	87°

TABLE II. Contact angle obtained for different slabs types: ϵ_{GT}, q_{GT} represent the GT model surface as defined in table I. $1\%\epsilon_{GT}, q_{GT}$ represents the GT model in which ϵ of each atoms is reduced to 1% of the original value in the GT model; $\epsilon_G, (q = 0)$ stands for a slab without partial charges assigned to atoms but with LJ sites corresponding to the GT model

In the following, we evaluate the influence of the different types of interaction on the contact angle, since previous investigations^{38,39} have shown that the VdW interaction plays an important role in the adhesion of biomolecules on surfaces, in particular silica surfaces. To this purpose, we evaluated the contact angle for the case where the partial charges of silica atoms were set to 0 (this means no electrostatic interaction between water and silica), and for the case where the LJ interaction was reduced to 1 percent of its original strength. Table II compares the resulting contact angles for different slab thickness.

It is interesting to see that without partial charges, one obtains a contact angle of 105° for thin slabs, which means that the surface has become hydrophobic, with $\gamma_2/\gamma_1 \simeq 0.26$. But it becomes slightly hydrophilic when the slab is thicker, and this change in the hydroaffinity must be due to the VdW interaction.

In the opposite case, where the VdW interaction is reduced the surface is highly hydrophilic ($\theta = 11.1^\circ$), even though it is not as hydrophilic as with the VdW interaction. This means that the electrostatic interaction influences the wetting properties more than the VdW interaction.

V. CONCLUSION

We have investigated the wetting properties of water in partially filled silica pores and on flat silica surfaces using MD simulations with two widely used intermolecular potentials^{34,36} for the interaction of water and silica surface atoms. This investigation was made possible since we have developed a method for constructing realistic silica slabs⁴⁴, with uniformly distributed silanol groups on the surface. The study was motivated by experimental findings that water in partially filled silica pores

wets the surface completely.^{2,12} These experiments measured the absorption of water in MCM-41, SBA-15² and in CPG¹² pore material using ^1H -MAS solid state NMR spectroscopy. An evaluation of the ^1H chemicals shift of the water hydrogen atoms in the pore showed that the inner surface of the pore is at first completely covered during the filling mechanism, and with increasing filling ratio the center of the pore becomes filled. These experiments were used to measure the surface density of silanol groups on the pore surface.

The finding that water wets the pore surface completely was not retrieved in our first simulations using the standard BZ silica model.

Our comprehensive analysis shows that the GT silica model³⁶ surface is more hydrophilic than the standard BZ silica model³⁴ surface. This must be due to the different partial charges assigned to silica atoms in the two models, in agreement with our result shown in the last section that the electrostatic interaction plays a prominent role in the wetting properties of water on silica surfaces.

Based on the evaluation of radial and angular density profiles, we found that the GT silica model surface is completely covered by water molecules even at low filling ratios (30 %, 40 %), and that roughly one and a half layer of water is sufficient for a full wetting of the surface. This result does not show a dependence on the water models used and on the starting configuration of the water droplet inside the silica pore. For the BZ model surface, the arrangement of water in the pore depends on the filling ratio and on the starting configuration. A simple analytical evaluation of the possible water phases in a pore revealed that for the BZ model, the interfacial energy of the water droplet with the silica wall is smaller than the interfacial energy of water with vacuum, leading to water configurations that have small interfaces with the vacuum, while the opposite is true for the GT surface, where the interface with the silica surface is maximized. Near the BZ surface, we observed a formation of a double water layer at all filling ratios studied, agreeing well with the findings of other authors.^{29,30,32} However, our findings complement their work as we evaluated also the proportion of the pore surface that was wetted, and demonstrated the coexistence of different phases of water inside the pore at intermediate filling ratios. The occurring phases could not be fully explained by the phase diagram that was based solely on surface tensions, and we argued that the effect of entropy makes it plausible that the more compact "plug" phase is favored in the MD simulations. This conclusion finds support from MD simulation results^{19,31-33} (using again the BZ model) that for filling ratios ≤ 56 % water molecules within the first two layers from the substrate are in a glassy state even at room temperature, which means that they contribute little to the entropy.

In agreement with the different water arrangements found for the two potentials, we found that the contact angle of a water droplet wetting a silica slab is close to

zero for the GT silica model, while it is around 25° for the BZ model. Again, the GT model agrees well with experimental results.^{38,39} Furthermore, the contact angle decreases with slab thickness and reaches its limit at approximately $t = 2.5$ nm. This result matches well with the experimentally found value $t = 3$ nm³⁷ and can help in decreasing the computational cost of MD studies by limiting the thickness of the slab to $t = 3$ nm. Our simulations show also that the surface energy ratio γ_2/γ_1 is very close to -1 and can shift from a value > -1 (implying a finite contact angle) to a value < -1 (implying zero contact angle) with increasing thickness. Therefore small changes in the preparation of the silica surface can move the ratio over the threshold -1 and may explain why a nonzero contact angle is found in some experiments^{38,39} and complete wetting in others.^{2,12,37}

Finally, varying the LJ parameters and partial charges on the silica atoms, we found that tuning on the VdW interaction can make a hydrophobic non-polar surface slightly hydrophilic, underlining the important role of the VdW interaction found in experiments.^{38,39} However, electrostatic interactions play a dominant role for the wetting properties of water on polar surfaces.

ACKNOWLEDGMENTS

This work was supported by DFG grant number Dr300/11-2. It was also supported in part by Perimeter Institute for Theoretical Physics. Research at Perimeter Institute is supported by the Government of Canada through Industry Canada and by the Province of Ontario through the Ministry of Economic Development & Innovation.

- ¹A. Scodinu, and J. T. Fourkas, Comparison of the orientational dynamics of water confined in hydrophobic and hydrophilic nanopores, *J. Phys. Chem. B*, vol. 106, p. 10292, (2002). [Online]. Available: <http://dx.doi.org/10.1021/jp026349l>
- ²B. Grünberg, T. Emmmler, E. Gedat, I. Shenderovich, G. H. Findenegg, H.-H. Limbach, and G. Buntkowsky, Hydrogen bonding of water confined in mesoporous silica mcm-41 and sba-15 studied by 1h solid-state nmr, *Chem. Eur. J.*, vol. 10, p. 5689, (2004). [Online]. Available: <http://dx.doi.org/10.1002/chem.200400351>
- ³S. Takahara, M. Nakano, S. Kittaka, Y. Kuroda, T. Mori, H. Hamano, and T. Yamaguchi, Neutron scattering study on dynamics of water molecules in mcm-41, *J. Phys. Chem. B*, vol. 103, p. 5814, (1999). [Online]. Available: <http://dx.doi.org/10.1021/jp984136j>
- ⁴A. Faraone, L. Liu, C.-Y. Mou, P.-C. Shih, J. R. D. Copley, and S.-H. Chen, Translational and rotational dynamics of water in mesoporous silica materials: Mcm-41-s and mcm-48-s, *J. Chem. Phys.*, vol. 119, p. 3963, (2003). [Online]. Available: <http://dx.doi.org/10.1063/1.1584653>
- ⁵P. Smirnov, T. Yamaguchi, S. Kittaka, S. Takahara, and Y. Kuroda, X-ray diffraction study of water confined in mesoporous mcm-41 materials over a temperature range of 223-298 K, *J. Phys. Chem. B*, vol. 104, p. 5498, (2000). [Online]. Available: <http://dx.doi.org/10.1021/jp994326>
- ⁶S. Takahara, N. Sumiyama, S. Kittaka, T. Yamaguchi, and M.-C. Bellissent-Funel, Neutron scattering study on dynamics of water molecules in mcm-41. 2. determination of translational diffusion coefficient, *J. Phys. Chem. B*, vol. 109, p. 11231, (2005). [Online]. Available: <http://dx.doi.org/10.1021/jp046036l>
- ⁷S. Kittaka, S. Takahara, H. Matsumoto, Y. Wada, T. J. Satoh, and T. Yamaguchi, Low temperature phase properties of water confined in mesoporous silica mcm-41: Thermodynamic and neutron scattering study, *J. Chem. Phys.*, vol. 138, p. 204714, (2013). [Online]. Available: <http://dx.doi.org/10.1063/1.4807593>
- ⁸J.-C. LI, D. K. Ross, and M. J. BENHAM, Small-angle neutron scattering studies of water and ice in porous vycor glass, *J. Appl. Cryst.*, vol. 24, p. 794, (1991). [Online]. Available: <http://dx.doi.org/10.1107/S0021889891001929>
- ⁹F. Bruni, M. A. Ricci, and A. K. Soper, Water confined in vycor glass. i. a neutron diffraction study, *J. Chem. Phys.*, vol. 109, p. 1478, (1998). [Online]. Available: <http://dx.doi.org/10.1063/1.476698>
- ¹⁰H. Thompson, A. K. Soper, M. A. Ricci, F. Bruni, and N. T. Skipper, The three-dimensional structure of water confined in nanoporous vycor glass, *J. Phys. Chem. B*, vol. 111, p. 5610, (2007). [Online]. Available: <http://dx.doi.org/10.1021/jp0677905>
- ¹¹A. Vyalikh, T. Emmmler, E. Gedat, I. Shenderovich, G. H. Findenegg, H.-H. Limbach, G. Buntkowsky, Evidence of microphase separation in controlled pore glasses, *Solid State NMR*, vol. 28, p. 117, (2005). [Online]. Available: <http://dx.doi.org/10.1016/j.ssnmr.2005.07.001>
- ¹²A. Vyalikh, T. Emmmler, B. Grünberg, Y. Xu, I. Shenderovich, H. Findenegg, H.-H. Limbach, and G. Buntkowsky, Hydrogen bonding of water confined in controlled-pore glass 10-75 studied by 1h-solid state nmr, *Z. Phys. Chem.*, vol. 221, p. 155, (2007). [Online]. Available: <http://dx.doi.org/10.1524/zpch.2007.221.1.155>
- ¹³C. Alba-Simionesco, B. Coasne, G. Dosseh, G. Dudziak, K. E. Gubbins, R. Radhakrishnan, M. Sliwinski-Bartkowiak, Effects of confinement on freezing and melting, *J. Phys. Condens. Matter*, vol. 18, p. R15, (2006). [Online]. Available: <http://dx.doi.org/10.1088/0953-8984/18/6/R01>
- ¹⁴A. C. Fogarty, E. D.-Dijon, D. Laage, and W. H. Thompson, Origins of the non-exponential reorientation dynamics of nanoconfined water, *J. Chem. Phys.*, vol. 141, p. 18C523, (2014). [Online]. Available: <http://dx.doi.org/10.1063/1.4896983>
- ¹⁵W. H. Thompson, title = Solvation Dynamics and Proton Transfer in Nanoconfined Liquids, *Annu. Rev. Phys. Chem.*, vol. 62, p. 599, (2011). [Online]. Available: <http://dx.doi.org/10.1146/annurev-physchem-032210-103330>
- ¹⁶M. F. Harrach, F. Klameth, B. Drossel, and M. Vogel, Effect of the hydroaffinity and topology of pore walls on the structure and dynamics of confined water, *J. Chem. Phys.*, vol. 142, p. 034703, (2015). [Online]. Available: <http://dx.doi.org/10.1063/1.4905557>
- ¹⁷J. C. Fogarty, H. M. Aktulga, A. Y. Grama, A. C. T. van Duin, and S. A. Pandit, A reactive molecular dynamics simulation of the silica-water interface, *J. Chem. Phys.*, vol. 132, p. 174704, (2010). [Online]. Available: <http://dx.doi.org/10.1063/1.3407433>
- ¹⁸I. Brovchenko, A. Geiger, A. Oleinikova, and D. Paschek, Phase coexistence and dynamic properties of water in nanopores, *Eur. Phys. J. E*, vol. 12, p. 69, (2003). [Online]. Available: <http://dx.doi.org/10.1140/epje/i2003-10028-4>
- ¹⁹P. Gallo, M. Rovere, M. A. Ricci, C. Hartnig, and E. Spohr, Evidence of glassy behaviour of water molecules in confined states, *Phil. Mag. Part B*, vol. 79, p. 1923, (1999). [Online]. Available: <http://dx.doi.org/10.1080/13642819908223078>
- ²⁰A. A. Milischuk, and B. M. Ladanyi, Polarizability anisotropy relaxation in nanoconfinement: Molecular simulation study of water in cylindrical silica pores, *J. Chem. Phys.*, vol. 141, p. 18C513, (2014). [Online]. Available: <http://dx.doi.org/10.1021/jp4064615>
- ²¹R. Renou, A. Szymczyk, and A. Ghofri, Tunable dielectric constant of water at the nanoscale, *Phys. Rev. E*, vol. 91, p. 032411, (2015). [Online]. Available: <http://dx.doi.org/10.1103/PhysRevE.91.032411>
- ²²H. Zhang, A. A. Hassanali, Y. K. Shin, C. Knight, and S. J. Singer, The water amorphous silica interface: Anal-

- ysis of the stern layer and surface conduction, *J. Chem. Phys.*, vol. 134, p. 024705, (2011). [Online]. Available: <http://dx.doi.org/10.1063/1.3510536>
- ²³B. Berkowitz, Characterizing flow and transport in fractured geological media: A review, *Adv. Water Res.*, vol. 25, p. 861, (2002). [Online]. Available: [http://dx.doi.org/10.1016/S0309-1708\(02\)00042-8](http://dx.doi.org/10.1016/S0309-1708(02)00042-8)
- ²⁴H. A. Stone, A. D. Stroock, and A. Ajdari, Engineering flows in small devices microfluidics toward a lab-on-a-chip, *Annu. Rev. Fluid Mech.*, vol. 36, p. 381, (2004). [Online]. Available: <http://dx.doi.org/10.1146/annurev.fluid.36.050802.122124>
- ²⁵A. Corma, S. Iborra, and A. Velty, Chemical routes for the transformation of biomass into chemicals, *Chem. Rev.*, vol. 107, p. 2411, (2007). [Online]. Available: <https://www.pharosproject.net/uploads/files/cml/1393448498.pdf>
- ²⁶S. Berneche, and B. Roux, Energetics of ion conduction through the K⁺ channel, *Nature*, vol. 414, p. 73 (2001). [Online]. Available: <http://dx.doi.org/10.1038/35102067>
- ²⁷M. A. Ricci, F. Bruni, P. Gallo, M. Rovere, and A. K. Soper, Water in confined geometries: experiments and simulations, *J. Phys. Condens. Matter*, vol. 12, p. A345, (2000). [Online]. Available: <http://dx.doi.org/10.1088/0953-8984/12/8A/346>
- ²⁸J. Jelassi, T. Grosz, I. Bako, M.-C. Bellissent-Funel, J. C. Dore, H. L. Castircum, and R. Sridi-Dorbez, Structural studies of water in hydrophilic and hydrophobic mesoporous silicas: An x-ray and neutron diffraction study at 297 K, *J. Chem. Phys.*, vol. 134, p. 064509, (2011). [Online]. Available: <http://dx.doi.org/10.1063/1.3530584>
- ²⁹C. Hartnig, W. Witschel, E. Spohr, P. Gallo, M. A. Ricci, M. Rovere, Modification of the hydrogen bond network of liquid water in a cylindrical SiO₂ pore, *J. Mol. Liq.*, vol. 85, p. 127, (2000). [Online]. Available: <https://arxiv.org/abs/cond-mat/0002453>
- ³⁰E. Spohr, C. Hartnig, P. Gallo, M. Rovere, Water in porous glasses: a computer simulation study, *J. Mol. Liq.*, vol. 80, p. 165, (1999). [Online]. Available: [http://dx.doi.org/10.1016/S0167-7322\(99\)80006-3](http://dx.doi.org/10.1016/S0167-7322(99)80006-3)
- ³¹P. Gallo, M. Rovere, and S-H Chen, Anomalous dynamics of water confined in mcm-41 at different hydrations, *J. Phys. Condens. Matter*, vol. 22, p. 284102, (2010). [Online]. Available: <http://dx.doi.org/10.1088/0953-8984/22/28/284102>
- ³²P. Gallo, M. Rovere, and E. Spohr, Glass transition and layering effects in confined water: A computer simulation study, *J. Chem. Phys.*, vol. 113, p. 11324, (2000). [Online]. Available: <http://dx.doi.org/10.1063/1.1328073>
- ³³P. Gallo, M. Rovere, M. A. Ricci, C. Hartnig, and E. Spohr, Non-exponential kinetic behaviour of confined water, *Europhys. Lett.*, vol. 49, p. 183, (2000). [Online]. Available: <http://dx.doi.org/10.1209/epl/i2000-00132-1>
- ³⁴A. Bródka, and T. W. Zerda, Properties of liquid acetone in silica pores: Molecular dynamics simulation, *J. Chem. Phys.*, vol. 104, p. 6319, (1996). [Online]. Available: <http://dx.doi.org/10.1063/1.471292>
- ³⁵H. Margenau, and N. R. Kestner, *Theory of Intermolecular Forces*. Pergamon, Oxford, 1969.
- ³⁶T. S. Gulmen, and W. H. Thompson, Testing the two-state model of nanoconfined liquids: The conformational equilibrium of ethylene glycol in amorphous silica pores, *Lang.*, vol. 22, p. 10919, (2006). [Online]. Available: <http://dx.doi.org/10.1021/la062285k>
- ³⁷R. Williams, and A. M. Goodman, Wetting of thin layers of sio₂ by water, *App. Phys. Lett.*, vol. 25, p. 531, (1974). [Online]. Available: <http://dx.doi.org/10.1063/1.1655297>
- ³⁸M. Lessel, P. Loskill, F. Hausen, N. N. Gosvami, R. Bennewitz, and K. Jacobs, Impact of van der Waals interactions on single asperity friction, *Phys. Rev. Lett.*, vol. 111, p. 035502, (2013). [Online]. Available: <http://dx.doi.org/10.1103/PhysRevLett.111.035502>
- ³⁹P. Loskill, H. Hähl, T. Faidt, S. Grandthyll, F. Müller, and K. Jacobs, Is adhesion superficial? silicon wafers as a model system to study van der Waals interactions, *Adv. Coll. Inter. Sci.*, vol. 179, p. 107, (2012). [Online]. Available: <https://arxiv.org/abs/1202.6304v1>
- ⁴⁰E. R. Cruz-Chu, A. Aksimentiev, and K. Schulten, Water-silica force field for simulating nanodevices, *J. Phys. Chem. B*, vol. 110, p. 21497, (2006). [Online]. Available: <http://dx.doi.org/10.1021/jp063896o>
- ⁴¹F. S. Emami, V. Puddu, R. J. Berry, V. Varshney, S. V. Patwardhan, C. C. Perry, and H. Heinz, Force field and a surface model database for silica to simulate interfacial properties in atomic resolution, *Chem. Mater.*, vol. 26, p. 2647, (2014). [Online]. Available: <http://dx.doi.org/10.1021/cm500365c>
- ⁴²R. Seemann, S. Herminghaus, C. Neto, S. Schlagowski, D. Podzimek, R. Konrad, H. Mantz, and K. Jacobs, Dynamics and structure formation in thin polymer melt films, *J. Phys. Condens. Matter*, vol. 17, p. 267, (2005). [Online]. Available: <http://dx.doi.org/10.1088/0953-8984/17/9/001>
- ⁴³J. C. Phillips, R. Braun, W. Wang, J. Gumbart, E. Tajkhorshid, E. Villa, C. Chipot, R. D. Skeel, L. Kale, and K. Schulten, Scalable molecular dynamics with namd, *J. Comput. Chem.*, vol. 26, p. 1781, (2005). [Online]. Available: <http://dx.doi.org/10.1002/jcc.20289>
- ⁴⁴J. Geske, and M. Vogel, Creating realistic silica nanopores for molecular dynamics simulations, (unpublished).
- ⁴⁵J.-R. Hill, and J. Sauer, Molecular mechanics potential for silica and zeolite catalysts based on ab initio calculations. 1. dense and microporous silica, *J. Phys. Chem.*, vol. 98, p. 1238, (1994). [Online]. Available: <http://dx.doi.org/10.1021/j100055a032>
- ⁴⁶H. J. C. Berendsen, J. R. Grigera, and T. P. Straatsma, The missing term in effective pair potentials, *J. Phys. Chem.*, vol. 91, p. 6269, 1987. [Online]. Available: <http://dx.doi.org/10.1021/j100308a038>
- ⁴⁷J. L. F. Abascal, and C. Vega, A general purpose model for the condensed phases of water: Tip4p/(2005), *J. Chem. Phys.*, vol. 123, p. 234505, (2005). [Online]. Available: <http://dx.doi.org/10.1063/1.2121687>
- ⁴⁸W. Humphrey, A. Dalke, and K. Schulten, Vmd: Visual molecular dynamics, *J. Mol. Graphics*, vol. 14, p. 33, (1996). [Online]. Available: <http://www.ks.uiuc.edu/Research/vmd/>